Biochimica et Biophysica Acta 1837 (2014) 940–952

Contents lists available at ScienceDirect

Biochimica et Biophysica Acta

journal homepage: www.elsevier.com/locate/bbabio

Review

ATP synthases from archaea: The beauty of a molecular motor

Gerhard Grüber [a,*], Malathy Sony Subramanian Manimekalai [a], Florian Mayer [b], Volker Müller [b,*]

[a] School of Biological Sciences, Nanyang Technological University, 60 Nanyang Drive, Singapore 637551, Republic of Singapore
[b] Molecular Microbiology & Bioenergetics, Institute of Molecular Biosciences, Johann Wolfgang Goethe University Frankfurt/Main, Max-von-Laue-Str. 9, 60438 Frankfurt, Germany

ARTICLE INFO

Article history:
Received 13 November 2013
Received in revised form 7 March 2014
Accepted 11 March 2014
Available online 17 March 2014

Keywords:
ATPase
Na^+ bioenergetics
Energy conservation
Methanogenesis
Rotary enzyme
c ring

ABSTRACT

Archaea live under different environmental conditions, such as high salinity, extreme pHs and cold or hot temperatures. How energy is conserved under such harsh environmental conditions is a major question in cellular bioenergetics of archaea. The key enzymes in energy conservation are the archaeal A_1A_O ATP synthases, a class of ATP synthases distinct from the F_1F_O ATP synthase ATP synthase found in bacteria, mitochondria and chloroplasts and the V_1V_O ATPases of eukaryotes. A_1A_O ATP synthases have distinct structural features such as a collar-like structure, an extended central stalk, and two peripheral stalks possibly stabilizing the A_1A_O ATP synthase during rotation in ATP synthesis/hydrolysis at high temperatures as well as to provide the storage of transient elastic energy during ion-pumping and ATP synthesis/-hydrolysis. High resolution structures of individual subunits and subcomplexes have been obtained in recent years that shed new light on the function and mechanism of this unique class of ATP synthases. An outstanding feature of archaeal A_1A_O ATP synthases is their diversity in size of rotor subunits and the coupling ion used for ATP synthesis with H^+, Na^+ or even H^+ and Na^+ using enzymes. The evolution of the H^+ binding site to a Na^+ binding site and its implications for the energy metabolism and physiology of the cell are discussed.

1. Introduction

Life under extreme conditions — some like it salty, some acidic, some cold or hot! Adaptation of archaea to different environmental conditions requires special cellular adaptation mechanisms to confer life and stability of proteins at temperatures at or above 100 °C, at salt concentrations up to 5 M or at pHs ranging from 1 to 12. Ever since archaea have been isolated, especially the hyperthermophilic archaea have attracted much interest. Hyperthermophilic organisms, which are defined as having optimal growth temperatures above or at 80 °C, were discovered over 30 years ago [1]. Since then more than 70 hyperthermophilic species have been isolated. The world records in growth at high temperatures are held by *Pyrococcus furiosus*, which grows at an optimal temperature of 100 °C [2], *Pyrodictium occultum*, which grows from 98 °C to 105 °C [3], *Hyperthermus butylicus*, which grows up to 108 °C [4], *Methanopyrus kandleri*, which grows up to 113 °C [5] and *Pyrolobus fumarii*, which grows between 90 °C and 113 °C (at a pressure of 25.000 kPa) and that can also withstand autoclaving at 121 °C [6]. So far no hyperthermophilic organism has yet been discovered growing at temperatures above 121 °C, but their existence is not impossible. Hyperthermophiles are the deepest branching organisms of the bacterial and archaeal 16S rRNA-based phylogenetic trees and are considered therefore to represent "early organisms" adapted to the conditions similar to those found on the early earth [1,7–10]. Hyperthermophiles were isolated from geothermally heated environments like submarine hydrothermal vents, from the walls of "black smoker" hydrothermal vent chimneys, hot marine sediments or hot springs, where hydrogen gas is found at high levels due to volcanic outgassing [11–15] or by abiotic production [11,16].

This review will introduce the strategies of energy conservation in archaea and the key component in cellular bioenergetics, the A_1A_O ATP synthase. Unlike energy conservation mechanism in eukaryotes and bacteria, in archaea, like methanogens, metabolism is coupled to the generation of a H^+- and/or Na^+-gradient across the membrane, and both ion gradients drive the synthesis of ATP [17]. The A_1A_O ATP synthase, catalyzing the synthesis of ATP, is composed of nine subunits in a proposed stoichiometry of A_3:B_3:C:D:E_2:F:H_2:*a*:c_x. The enzyme possesses a water-soluble A_1 sector, containing the catalytic sites, and an integral membrane A_O domain, involved in ion translocation [18]. A variety of structural approaches have given a deeper insight into the structural details of individual A_1A_O ATP synthase subunits as well as subcomplexes, and have revealed important evolutionary structural details that lead to variations in nucleotide recognition and mechanism of ATP synthesis and/or ATP hydrolysis of the biological nanomachine A_1A_O ATP synthase, when compared with the evolutionary related F_1F_O ATP synthases and eukaryotic V_1V_O ATPases.

* Correspondence to: G. Grüber, School of Biological Sciences, Nanyang Technological University, Singapore 637551, Republic of Singapore. Tel.: +65 6316 2989; fax: +65 6791 3856 and V. Müller, Molecular Microbiology & Bioenergetics, Institute of Molecular Biosciences, Johann Wolfgang Goethe University Frankfurt/Main, Max-von-Laue-Str.9, 60438 Frankfurt, Germany. Tel.: +49 69 79829507; fax: +49 69 79829306.
E-mail addresses: ggrueber@ntu.edu.sg (G. Grüber), vmueller@bio.uni-frankfurt.de (V. Müller).

http://dx.doi.org/10.1016/j.bbabio.2014.03.004
0005-2728/

2. Energy conservation in archaea

The principle mechanisms of energy conservation known to date, e. g. chemiosmosis or substrate level phosphorylation (SLP) were invented very early in evolution and are found also in archaea, but due to their phylogenetic position, very close to the root of the tree of life, it is hypothesized that ancient forms of chemiosmosis are present in archaea [19]. Up to now five phyla are present in the domain *Archaea*. The *Euryarchaeota*, containing methanogens, hyperthermophilic and halophilic archaea, and *Crenarchaeota* with archaea having a sulfur metabolism (including some hyperthermophiles), are the two major phyla of *Archaea*. *Thaumarchaeota* are closely related to the *Crenarchaeota* and contain ammonia-oxidizing archaea. The phyla *Nanoarchaeota* and *Korarchaeota* are represented only by one species *Nanoarchaeum equitans* and *Korarchaeum cryptofilum*, respectively which are very close to the root of the tree of life. Archaea are physiologically enormously heterogeneous. They can grow heterotrophically on various compounds and use substrate level phosphorylation (SLP) to synthesize ATP in combination with chemiosmosis. Under anaerobic conditions energy can be conserved by fermentation, anaerobic respiration with nitrate, anaerobic photorespiration using bacteriorhodopsin as well as proton-pumping hydrogenases and sodium ion-pumping methyltransfer reactions [19,20]. Especially the hydrogenases are of great interest since hydrogen certainly was around in early earth and is used by a number of archaea as an electron donor. In the following section a brief introduction to hydrogen-dependent energy conservation mechanisms will be given. For more comprehensive reviews, the reader is referred to recent reviews [20–22].

P. furiosus, a hyperthermophilic strictly anaerobic archaeon that belongs to the phylum *Euryarchaeota*, conserves energy for growth by fermentation of carbohydrates and peptides to CO_2, H_2 and organic acids, e.g. acetate, in the absence of elemental sulfur [2]. Hydrogen is evolved by hydrogenases with reduced ferredoxin as an electron donor. Ferredoxin plays a central role in the energy metabolism of many anaerobic archaea (and bacteria). It has a redox potential well below −400 mV, up to −500 mV, and thus can be used to reduce protons to hydrogen gas ($E^{0\prime} = -414$ mV). This exergonic reaction is used to pump ions out of the cell, most likely Na^+, and the electrochemical Na^+ gradient established is then used to drive ATP synthesis [21]. This multisubunit membrane-bound hydrogenase (Mbh) has eight subunits comprising a hydrogen-oxidizing module as well as Na^+/H^+ antiporter modules [22]. Thus, for the subunit composition the Mbh resembles modern complex I enzymes and indeed, hydrogenases are the evolutionary precursor of complex I found in mitochondria or bacterial membranes. In *P. furiosus*, the hydrogenase is used to generate an electrochemical ion potential ($\Delta\tilde{\mu}_{Na}{}^{+}$) for transport processes and other energy-consuming membrane reactions but most of the cellular ATP is generated by substrate level phosphorylation during glycolysis [21]. This is different in *Thermococcus onnurineus* that can grow by oxidation of formate to carbon dioxide and hydrogen. This reaction is close to the thermodynamic equilibrium and actually is the reaction with the lowest ΔG known to sustain life (−2.6 kJ/mol) [23,24]. The reaction sequence is simple and involves a formate dehydrogenase that oxidizes formate and channels electrons to a membrane-bound hydrogenase, very similar to the enzyme described above for *P. furiosus* [22,23]. Electron transfer to protons leads to the generation of an ion gradient that then drives ATP synthesis. Although this has not been addressed experimentally, ATP synthesis is suggested to involve Na^+ as a coupling ion.

A unique pathway that allows growth under strictly anaerobic conditions is methanogenesis. Methanogens use only chemiosmosis for energy conservation and couple methanogenesis to the generation of two primary ion gradients [25]. One of these ion gradients is a primary, electrochemical sodium ion gradient established by the methyltetrahydromethanopterin–coenzyme M methyltransferase (Mtr) [26,27]. This reaction is common to every methanogen. Some methanogens also have an additional electron transport chain(s) that includes cytochromes and have evolved a second, additional mechanism to energize their membranes. This proton-motive electron transport chain leads to a heterodisulfide of coenzyme M and coenzyme B as an electron acceptor [28,29]. Therefore, methanogenic archaea, which have a methyltetrahydromethanopterin–coenzyme M methyltransferase (Mtr) and a proton-motive electron transport chain with cytochromes, couple methanogenesis to a proton and a sodium ion gradient at the same time [30].

3. ATP synthases from archaea

Despite all the differences in how the electrochemical ion potential to drive ATP synthesis is generated, all archaea have an ATP synthase. The enzyme catalyzes ATP synthesis according to Eq. (1), at the expense of the transmembrane electrical ion gradient [31,32]:

$$\mathrm{ADP} + \mathrm{P_i} + n\ \mathrm{ions_{out}} \leftrightarrow \mathrm{ATP} + n\ \mathrm{ions_{in}}. \quad (1)$$

Since the bioenergetics of archaea has such a wide variety of different mechanisms it was thought that the ATP synthases of archaea are different in different tribes! The activity of ATP synthases is rather easy to analyze. ATP hydrolysis can be measured by phosphate release from ATP or ATP synthesis can be studied by artificial pH jumps in whole cells [33]. Thus, the presence of the enzyme was demonstrated rather early in time. The nature of the enzyme was then addressed by attempts to purify it from different sources. Interestingly, despite all the attempts in the 1970–1980s, there was no clear picture on the subunit composition of the archaeal ATP synthases. All enzyme preparations varied in polypeptide compositions and the idea arose, that ATP synthases from archaea differ in subunit composition and thus in structure and function. Genes had been isolated, but only single genes, not the entire collection that encodes the A_1A_O ATP synthase. This is due to the fact that genes had been isolated from *Crenachaeota* in which, as determined later by genome sequencing, the genes are spread over the genome [34]. In contrast, the euryarchaeon *Methanosarcina mazei* Gö1 contained all genes in a cluster, actually in an operon, and this allowed for the first time a proposal on the subunit composition and topology in A_1A_O ATP synthases [35]. These data indicate that the enzyme contains at least nine subunits. This was (much later) confirmed after the first "complete" enzymes had been isolated [36]. Early electron micrographs revealed that the A_1A_O ATP synthase is, like the F_1F_O ATP synthase and the V_1V_O ATP synthase, organized in two domains that are connected by stalks [35].

At the time of discovery of archaeal ATP synthases two classes of ATP synthases/ATPases were known. The F_1F_O ATP synthases present in bacteria, mitochondria and chloroplasts were evolved to synthesize ATP. On the other hand, organelles of eukaryotes need to be energized to drive, for example, transport processes. Since electron transport machineries are only found in mitochondria or chloroplasts, the other organelles are energized by ATP that is hydrolyzed according to Eq. (1). The ATPase that catalyzes this reaction was purified from those organelles and shown to have the same overall domain topology, with membrane domain and a cytoplasmic domain that are connected by stalks. Some of the subunits of the globular cytoplasmic domain of V_1V_O ATPases and F_1F_O ATP synthases like α/B or β/A shared a considerable sequence identity (20–30%), whereas other smaller subunits did not. Therefore, it was concluded that ATP synthases/ATPases arose from a common ancestor but evolved into different classes with distinct function (ATP synthesis vs. ATP hydrolysis) [32,37–40]. Since the first organellar ATPases were purified from vacuoles, this class of enzymes is now referred to as vacuolar V_1V_O ATPases. It should be pointed out that eukaryotes thus have two different ATPases/ATP synthases: a F_1F_O ATP synthase in mitochondria and chloroplasts and a V_1V_O ATPase in other organelles. For a long time, there was a clear view on the "ATP synthase/ATPase world" that had two "continents", the F_1F_O ATP synthase and the V_1V_O ATPase.

After the first biochemical, immunological and molecular studies researchers were puzzled to group the archaeal enzymes. They apparently had properties of enzymes from both classes. Sequence analysis revealed a close relationship of the A and B subunits to A and B of V_1V_O ATPases, respectively [41]. Since the primary sequence identity of A and B was higher to A and B from V_1V_O ATPase than β/α from F_1F_O ATP synthase, the archaeal enzyme was named V_1V_O ATPase and genes were annotated as genes encoding V_1V_O ATPase subunits. However, already at that time, Mukohata and Schäfer [42,43] argued that, although the archaeal ATP synthase shares features with both, V_1V_O ATPase and F_1F_O ATP synthase the enzyme is so different from the other two groups, that they should be grouped in a third class, the archaeal or A_1A_O ATP synthase. This is now clearly justified by the structural and mechanistic results, as discussed below, and functional studies. Whereas the F_1F_O ATP synthase catalyzes ATP synthesis at the expense of an electrochemical ion gradient, the eukaryal V_1V_O ATPase functions as an ATP-driven ion pump, unable to synthesize ATP under physiological conditions. The cellular function of archaeal ATP synthase and F_1F_O ATP synthase is to synthesize ATP by ion gradient-driven phosphorylation, but the reaction is reversible and they may also work as an ATP-driven ion pumps to generate an ion gradient under fermentative conditions.

4. Structure and catalytic mechanism of the A_1A_O ATP synthase

4.1. The overall arrangement of the A_1A_O ATP synthase

The A_1A_O ATP synthase is composed of subunits A–F, H, *a* and *c* in the proposed stoichiometry of A_3:B_3:C:D:E_2:F:H_2:*a*:c_x. Similar to the related bacterial F_1F_O ATP synthase (α$_3$:β$_3$:γ:δ:ε:a:b$_2$:c$_x$) it possesses a water-soluble A_1 domain, containing the catalytic sites, and an integral membrane A_O domain, involved in ion translocation (Fig. 1A). Two dimensional- [44,45] and three dimensional reconstructions [46–48] of electron micrographs revealed a bipartite structure, consisting of A_1 and A_O domains, which form a pair of coupled rotary motors connected with one central and two peripheral stalks. The soluble A_1 domain has the catalytic activity and the hydrophobic membrane-embedded A_O domain is responsible for ion translocation across the membrane. A collar-like structure located perpendicular to the membrane seems to anchor the two peripheral stalks, which are not penetrating into the A_O domain. Both peripheral stalks go all the way up to the top of the A_3B_3 headpiece, thereby connecting statically and mechanistically the A_1 with the A_O sector via the collar-like domain.

4.2. High resolution structures of the nucleotide binding subunits A and B

The A_1 sector (A_1 ATPase) consists of the subunits A, B, C, D and F in the stoichiometry of A_3:B_3:C:D:F and is able to catalyze ATP hydrolysis [40]. In the last decade all individual subunits of the A_1 ATPase have been solved at high resolution [49–55]. Firstly, low resolution structures of the A_1 sector [56,57] and the entire A_1A_O ATP synthase [45–48], combined with cross-linking data [58,59], and later crystallographic structures of the A_3:B_3- [54] and A_3:B_3:D:F-complex [55] enabled the assignment into the enzyme complex shown in Fig. 1A–C. The headpiece of A_1 consists of the subunits A and B, alternating around the periphery of a central cavity, which is made up by subunit D. This central subunit penetrates inside this cavity and is in proximity to an A-B-A triplet [52,54–56], thereby coupling ion-translocation in the *a*–*c* interface of A_O with catalytic events in the ATP synthesizing interface of subunits A–B. Subunit A has been regarded as having catalytic function, while subunit B plays an important role in nucleotide binding and/or regulatory function [50,59]. Crystallographic structures of the nucleotide-binding subunits A [49,54,55] and B [50,54,55] of A_1A_O ATP synthases show that they are composed of an N-terminal β-barrel, an α–β central domain, and a C-terminal α-helical bundle, similar to the homologue nucleotide-binding subunits α and β of F_1F_O ATP synthases [60]. However, the superimposition of the two catalytic subunits of A and β of A_1A_O ATP synthases and F_1F_O ATP synthases, respectively,

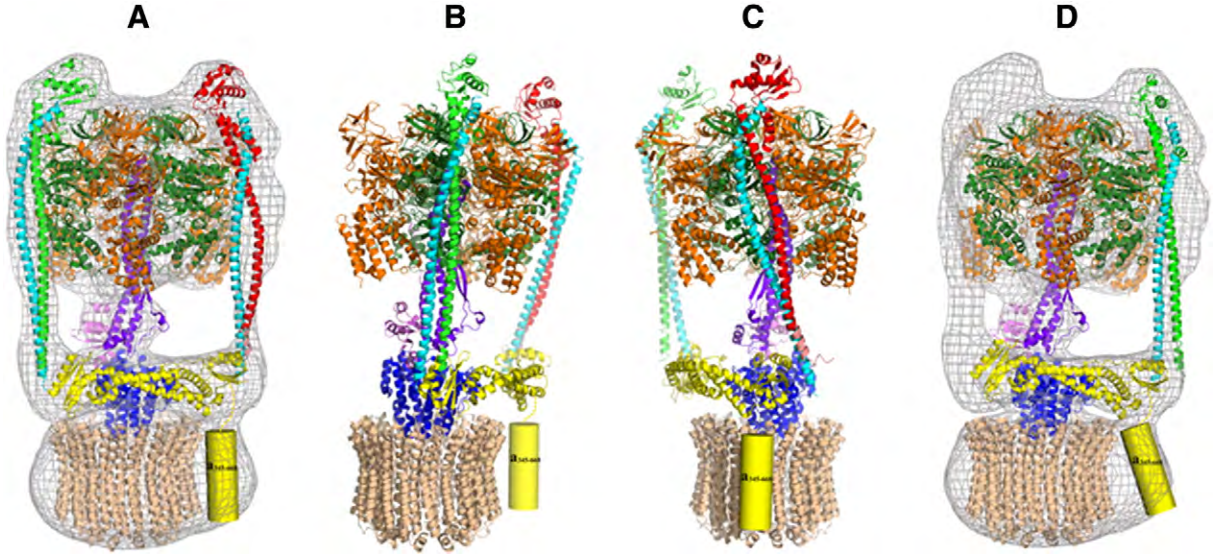

Fig. 1. (A–D) Arrangements of the atomic structures of A_1A_O ATP synthase subunits inside the EM map of archaeon *Pyrococcus furiosus* (EM Database ID: EMD 1542 [47]). Subunits A (orange) and B (dark green) from *Enterococcus hirae* (PDB ID: 3VR2 [55]) alternate in the A_3B_3 hexamer. The NMR structure of subunit F (PDB ID: 2OV6 [53]; *magenta*) and the crystal structure of subunit C (PDB ID: 1R5Z [51]; *blue*) and D (PDB ID: 3AON [52]; purple) form the central stalk. The structure of subunit *a* (yellow) was taken from PDB ID: 3RRK [81] and the *c* ring (*wheat*) from PDB ID: 2BL2 [96]. The *Thermus thermophilus* EH dimer (green and cyan) was taken from PDB ID: 3K5B [77] and reveals the almost straight peripheral stalk (B), whereas the crystal structure of *Pyrococcus horikoshii* OT3 subunit E (PDB ID: 4DT0 [79]; red) and the *T. thermophilus* structure form the kinked second peripheral stalk (*C*). It has been proposed [79] that ion-translocation in the interface of the *c* ring and the C-terminal membrane-embedded domain of subunit *a* (yellow cylinder) causes alterations in the A_O sector, which are transferred to the barbelled-shaped N-terminal domain of subunit a (yellow) and subunit C. As one consequence, the subunit *a* alterations will force the peripheral stalk subunits to switch from a more extended (D) into a curved conformation (A) and vice versa, providing the storage of transient elastic energy during ion-pumping and ATP synthesis/-hydrolysis (D). For clarity the EM map is not shown in figures B and C, while in figure D one of the peripheral stalk subunits is removed.

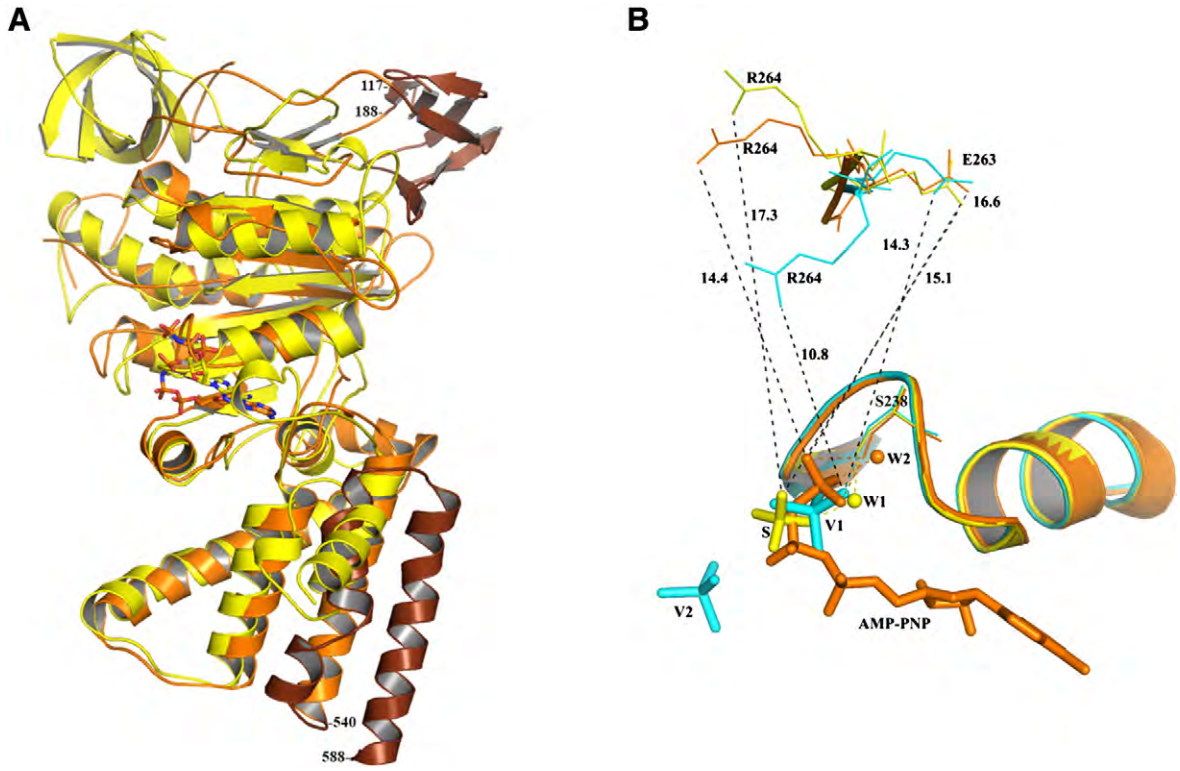

Fig. 2. (A) Structure comparison of the bovine β subunit (yellow; PDB ID: 1BMF [60]) and the AMP–PNP bound subunit A structure (orange; PDB ID: 3I4L [49]). Subunit A has two distinct structural features compared to β subunit which are highlighted in brown color; the non-homologues region (NHR from 117 to 188) and the C-terminal two helix extension from 540 to 588 residues. The difference in the binding of the AMP–PNP molecules could also be clearly noted. (B) Structure comparison of vanadate (A_{Vi}, *cyan*; PDB ID: 3P20 [66]), sulfate (A_S, yellow; PDB ID: 3I72 [49]) and AMP–PNP (A_{PNP}, orange; PDB ID: 3I4L [49]) bound structures of subunit A. The sheet-loop-helix motif of the P-loop is shown in cartoon representation. The various modes of interaction of the bound sulfate, vanadate and AMP–PNP molecules to the S238 residues in the A_S, A_{Vi} and A_{PNP} structures are shown. The crucial water molecules are shown in sphere representation. The water molecule from the A_S structure is marked as W1 and the one from A_{PNP} is marked as W2. The sulfate (yellow stick) bound structure (A_S) is assumed to be in a substrate-binding-like state, the vanadate- (V1, cyan stick) bound structure (A_{Vi}) is proposed to take a transition like state, and the AMP–PNP- (orange stick) bound structure (A_{PNP}) the product-bound state. The S238 residue plays an important role by way of interacting with the ligand molecules in different modes in all states. The substrate-binding-like state and the product-release state are hydrated while the transition-like state is deprived of water molecules in the active site. The distances between the closest oxygen atom of the sulfate, vanadate and γ-phosphate of the AMP–PNP molecules to the GER-loop residues E263 and R264 for the A_S, A_{Vi} and A_{PNP} structures are also indicated. The second vanadate (V2, cyan stick) is also shown which demonstrates the pathway of entry of the substrate molecule.

shows differences in the subunits with the additional α-helices at the very C-terminus of subunit A and the so-called non-homologous region (NHR), of about 90 amino acids near the N-terminus [49] (Fig. 2A), which are not present in β subunits of F_1F_O ATP synthases, but present in subunit A of the related eukaryotic V_1V_O ATPases [61,62].

In comparison, as shown in the crystal structure of the *M. mazei* Gö1 A_1A_O ATP synthase B subunit [50], the peptides G13 to P23 of the N-terminus of subunit B forms a β-sheet-loop structure, and is homologous to the actin-binding motif of subunit B of the human V_1V_O ATPase. Whether the A_1 headpiece is linked with the actin network via subunit B, as described for the V_1V_O ATPase [63], has to be resolved.

4.3. Critical residues in the P-loop of the catalytic A subunit

Recently, the structure of the catalytic subunit A of the *Pyrococcus horikoshii* OT3 A_1A_O ATP synthase of the sulfate (A_S), ADP (A_{ADP}) and AMP–PNP (A_{PNP}) bound forms has been determined [49]. The results demonstrated that the phosphate binding loop (P-loop) residue serine is highly important for the interaction with the nucleotides and the inorganic phosphate (Fig. 2B). Reflected also by the diverse P-loop sequence, the crystallographic structures indicated that subunit A has a unique arched conformation for the P-loop region, due to which the mode of binding of the nucleotide is different from that of the catalytic β-subunit of F_1F_O ATP synthases. The second unique P-loop residue in subunit A, phenylalanine, stabilizes this arched loop (Fig. 2B) and is therefore one of the critical residues in the P-loop sequence (GPFGSGKT) of subunit A. This phenylalanine residue is the equivalent amino acid to the alanine in subunit β of F_1F_O ATP synthases (GGAGVGKT), which is a key residue in the catalytic process inside the β subunit that moves towards the γ-phosphate of ATP during catalysis [60].

The different amino acid composition in the P-loop of subunit β of F_1F_O ATP synthases is also reflected by its horizontal orientation. The novel P-loop conformation in subunit A forces the nucleotide into a different arrangement inside the catalytic site with weaker interactions of different and/or homologous surrounding amino acid residues and making the nucleotide more solvent exposed [49]. This structural feature explains the ability of A_1A_O ATP synthases to hydrolyze apart from ATP also GTP and UTP with 86% and 54% activities, respectively [64,65]. These structural designs demonstrate how nature optimizes biological activities down to such tiny details.

The importance of the polar serine residue of the P-loop in subunit A is also indicated in the recently determined structures of the sulfate A_S [49] and transition-like state, vanadate-bound form of catalytic subunit A (A_{Vi}) of the A_1A_O ATP synthase from *P. horikoshii* OT3 [64] (Fig. 2B). In both structures the sulfate or vanadate interacts only with S238 in the P-loop. However, the mode of interaction is very different; while in A_S it is through a water molecule, in A_{Vi} it is a direct hydrogen bonding interaction. A comparison of the A_{Vi}, A_S and AMP–PNP (A_{PNP}) bound structures showed that the vanadate molecule is positioned closer to the P-loop compared to the sulfate molecule, and that the γ-phosphate is placed even closer in the A_{PNP} structure, indicating that vanadate is situated in the intermediate position. By analogy with vanadate-bound structures of the biological motors F_1F_O ATP synthase and myosin [66,67] it could be interpreted that the

vanadate-bound state mimics a transition-like state, with the sulfate- (a phosphate mimic) bound structure (A_S) taking the substrate-like position and the AMP–PNP-bound structure (A_{PNP}) adopting the product-bound state during catalysis (Fig. 2B).

Structural rearrangement of catalytically important residues in the so-called Walker B motif of subunit A became obvious, when the A_{Vi}, A_S and A_{PNP} bound structures have been compared (Fig. 2B, [64]). The Walker B motif residues or GER-loop, which is located above the P-loop (Walker A motif) and known to be involved in immobilization and polarization of a water molecule to facilitate nucleophilic attack at the γ-phosphate of ATP, is deviated by around 3.2 Å in the A_{Vi} structure when compared with the A_S structure. Further, the side chains of glutamate (E263) and arginine (R264) residues are significantly deviated by 2.3 Å and 6.6 Å, respectively, moving closer to the vanadate molecule (Fig. 2B) and revealing substantial structural rearrangement during the catalytic event.

The A_{Vi} structure of the A_1A_O ATP synthase showed for the first time the entry of the substrate sulfate, a phosphate analogue, molecule into a catalytic subunit of an ATP synthase (Fig. 2B). A second vanadate molecule is found to be positioned, where the ATP molecule transiently associates in the B subunit structure [68], demonstrating a similar pathway of entry for both subunits in A_1A_O ATP synthases. This position also confirms the recent finding that during ATP synthesis the inorganic phosphate binds first and hinders ATP binding to the catalytic site, which then selectively allows binding of ADP [69].

4.4. How the nucleotide enters into the binding pocket

The crystal structures of the nucleotide bound subunit B of the A_1A_O ATP synthase from *M. mazei* Gö1 showed for the first time in ATP synthases, how the ATP traverses the protein surface via two transient intermediate binding sites to its final binding pocket and the concomitant rearrangements in the nucleotide-binding and C-terminal region of subunit B (Figs. 3A–B) [68,70,71]. When the nucleotide enters close to the C-terminal domain of B, subunit D moves slightly, paving way for it to interact with subunit B (transition state 1 in Fig. 3B), which makes the C-terminal domain rotate by 6°. This moves the nucleotide inside the A_3B_3 hexamer, close to P-loop of subunit B (transition state 2), a position which compares well with the binding site of the antibiotic, efrapeptin C in the β subunit of F_1F_O ATP synthases. Efrapeptin C

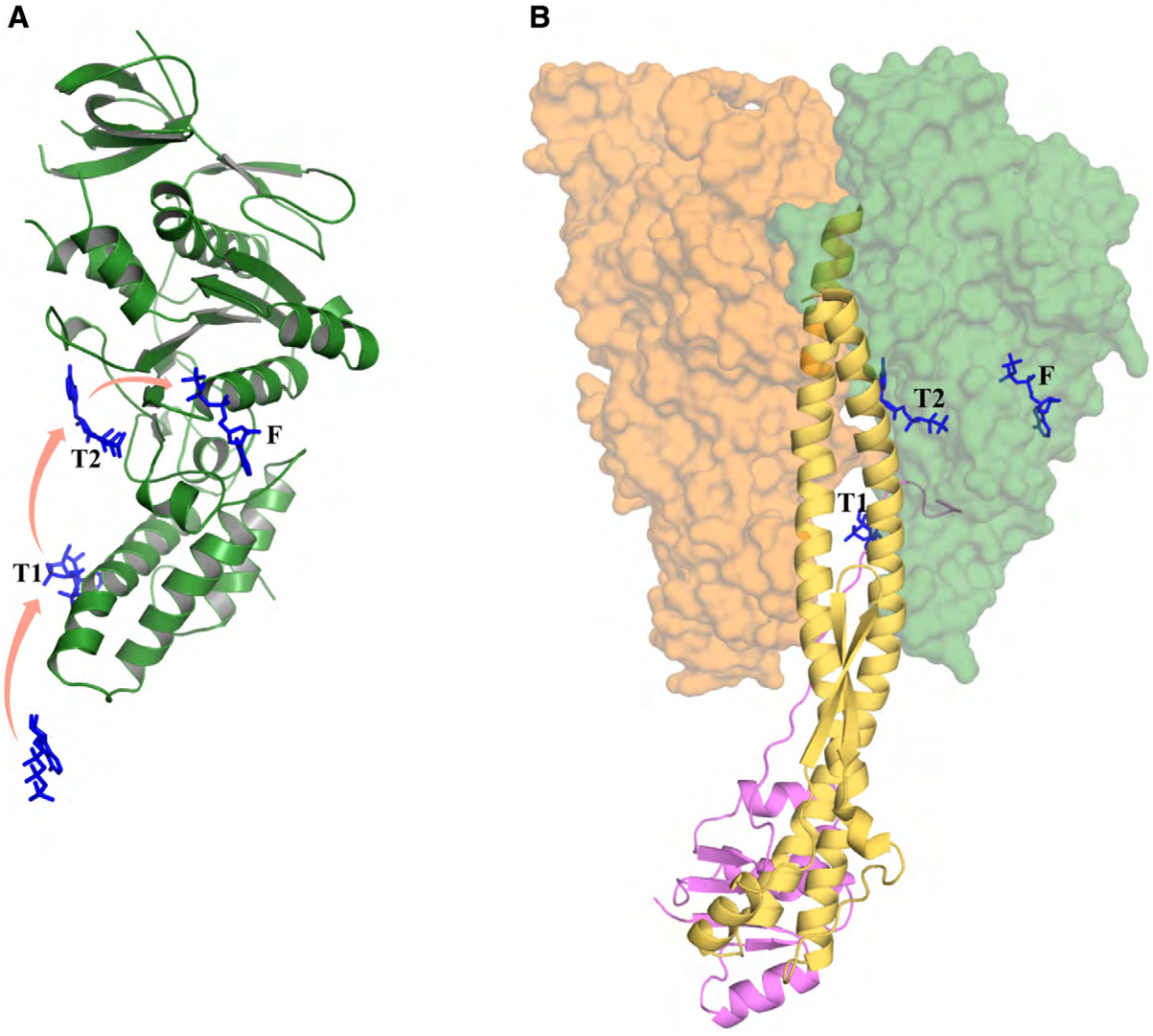

Fig. 3. (A) Structure of subunit B from *M. mazei* Gö1 (dark *green*) showing the different transition sites of the ATP molecule (blue stick). (*B*) Cross sectional view of the hexamer model of A_1A_O ATP synthase with subunits D (PDB ID: 3AON [52]; yellow) and F (PDB ID: 2OV6 [53]; magenta). Subunits B (*dark green*; PDB ID: 2C61 [50]) and A (*orange*; PDB ID: 3I4L [49]) are shown as surface representation. The ATP molecule enters via the gap formed by subunits A and B into the hexamer and positions in transient 1 (T1), whereby the C-terminal domain of subunit B rotates and allows the ATP molecule to penetrate into the hexamer in concert with the rotation of subunit D. A concerted movement of the C-termini of subunits B and F as well the rotation of D moves the nucleotide towards the transient 2 (T2), which is placed near to the P-loop, followed by the movement of ATP to the final binding site (F).

is a potent inhibitor of F_1F_O ATP synthases in mitochondria and some bacterial species [72]. Due to the rotational movement of the central stalk subunit D, the nucleotide will be moved to the actual binding site of subunit B [71].

4.5. The central stalk couples ion-translocation and ATP synthesis

The shape of the A_1 domain had shown that the A_3B_3 hexamer and the A_O sector are separated by a 80 Å long central stalk, consisting of the subunits C, D and F, with subunit C forming the bottom of the central stalk [45,57]. As shown by the crystallographic structure of the *Enterococcus hirae* subunit D, this protein comprises a long left-handed coiled coil structure with a unique short β-hairpin [52,55]. Such left handed coiled-coil structure is also conserved in the rotary proteins FliJ of the flagellar type III protein export apparatus [73] and subunit γ of F_1F_O ATP synthases [60]. In contrast, the β-hairpin region of subunit D is specific for this subunit and important for ATPase activity in A_1A_O ATP synthases [55]. Subunit D can be cross-linked to subunit A in a nucleotide-dependent manner [58]. The interaction between both subunits involves both N- and C-terminal segments of D.

Similarly, in *M. mazei* Gö1 A_1A_O ATP synthase, subunit F can be cross-linked to subunit B through their C-terminal sequences, which shows a nucleotide-dependent behavior [59]. The high resolution structure of B subunit revealed [50] that the C-terminal peptide of B is at a similar position to the so-called DELSEED-region of the nucleotide-binding subunit β of the F_1F_O ATP synthases [60], which also form a disulphide bond with the C-terminal helix of the coupling subunit γ. Subunit F in solution exhibits a distinct two-domain structure, with the N-terminal globular region having 78 residues and the residues 79–101 forming the flexible C-terminal part [53]. The flexible C-terminal tail enables this subunit to undergo up and down movements relative to subunit B, bringing both termini in close proximity (Fig. 3B). The DF- [52] and A_3B_3DF-crystal structures [55] of the *E. hirae* enzyme show that the four-stranded β-sheet in the N-terminal part of subunit F mediates the interaction with subunit D, forming together the rotor shaft. The recently postulated model of the rotation mechanism in the *E. hirae* A_3B_3DF-crystal structures [55] reveal that the DF-assembly induces a switch from a bindable form to the nucleotide-bound form in one AB-pair, while the DF interaction with a second subunit AB-pair causes the alteration from a bound form to a tight nucleotide-binding form [55]. The rotational dynamics of the *E. hirae* A_3B_3DF-complex have recently been confirmed in single molecule studies [74], showing that DF rotates unidirectional in a counterclockwise direction during ATP hydrolysis with a maximal rotation rate of about 73 ± 2 revolutions/s. In contrast to the thermophilic *Bacillus* PS3 F_1 ATPase, which shows three 120° steps, which can be further divided into substeps, the *E. hirae* A_3B_3DF-complex revealed only three pauses separated by 120° [74], indicating the distinct difference between both molecular motors.

The tip of the central stalk in A_1A_O ATP synthases is made-up by subunit C, which has a funnel shaped structure [51] with a central cavity, providing space for the D and F assembly (Fig. 1B). As revealed by the 9.7 Å resolution structure of the *Thermus thermophilus* enzyme, subunit C sits asymmetrically on the *c* ring without penetrating significantly in to the central pore of the *c* ring [48]. The function of subunit C, which is characteristic for A_1A_O ATP synthases, has been described of being a spacer unit that plays a role in coupling and rotational steps [75].

4.6. The peripheral stalks and its elastic features

The peripheral stalks are made up by the subunits E and H (Fig. 1A–C). Concerning their sequence and subunit composition the peripheral stalks of A_1A_O ATP synthases are the most divergent elements compared to their related F_1F_O ATP synthases or eukaryotic V_1V_O ATPases [76]. As shown by the crystallographic structure of subunit H of the *T. thermophilus* A_1A_O ATP synthase [77] this protein is entirely α-helical with a long N-terminal helix and a shorter C-terminal helix, which are linked by a sharp kink (Fig. 1A–D). This C-terminal helix is close to the N-terminal helix and the C-terminal tail of subunit E. The kink of subunit H together with the loop of subunit E are predicted to be two flexible joints that tether the headgroup to the coiled-coil region formed by the N-terminal helices of subunits E and H.

Subunit E is a long, two domain protein with a C-terminal globular domain [77–79], which is in close proximity to the top of an A–B interface and C-terminus of H (Fig. 1A), and an extended N-terminal α-helix. Structures of a straight- (*T. thermophilus*, [77]) and a S-shaped conformation (*P. horikoshii* OT3, [79]) of the extended N-terminal α-helix subunit E have been determined, which fit well into the asymmetric peripheral stalks of the 3D reconstruction of the *P. furiosus* enzyme [79] (Fig. 1B–C). These features support the model in which the switch from a straight- to an S-shaped conformation of subunit E in the two peripheral stalks facilitates elastic power transmission between the A_O and A_1 part, which is essential for facilitating the cooperation of the A_O and A_1 motors and to increase the kinetic efficiency of the A_1A_O ATP synthase engine [79,80]. Furthermore, it has been proposed [79] that ion-translocation in the interface of the *c* ring and the C-terminal membrane-embedded domain of subunit *a* causes alterations in the A_O sector (Fig. 1A, D), which are transferred to the barbell-shaped N-terminal domain of subunit *a* and subunit C. As a consequence, the subunit *a* alterations will force the peripheral stalk subunits to switch from a more extended (Fig. 1A, subunit E (green)) into a curved conformation (Fig. 1A, subunit E (red)) and *vice versa*, providing the storage of transient elastic energy during ion-pumping and ATP synthesis/-hydrolysis.

4.7. Architecture of the membrane-embedded A_O domain

The two peripheral stalks of A_1A_O ATP synthases, which have no membrane-spanning N-terminal helix like the one in F_1F_O ATP synthases, are linked to the globular domain of subunit *a*, whose C-terminal membrane-integrated segment forms the ion channel together with the *c* ring [47,48]. The A_1A_O ATP synthase subunit *a* (about 95 kDa) is similar to its related subunit *a* in eukaryotic V_1V_O ATPases and is partially functionally similar to subunit *a* (about 28 kDa) of F_1F_O ATP synthases [31]. Its C-terminal and ion-translocating part is membrane-integral and its N-terminal domain (about 40 kDa) is on the cytoplasmic side. The crystallographic structure of the barbell-shaped N-terminal domain of the *Meiothermus ruber* A_1A_O ATP synthase has been determined [81], (Fig. 1A–C). The middle and helical bundle of subunit *a* faces the wedge-like subunit C. The hydrophobic C-terminus of *a* is predicted to have 7–8 transmembrane helices and is known to be involved in ion translocation [47]. These α-helices are in close contact to a ring made by multiple copies of subunit *c*, the rotor subunit. Subunit *a* is suggested to form two "ion channels" to load the *c* ring with coupling ions over the first channel and to remove the ion again from the *c* ring over the second ion channel [48]. The recently determined 3-dimensional reconstruction of the *T. thermophilus* complex shows the eight transmembrane helices in subunit *a* [48]. These helices divide into two bundles, each containing four helices (Fig. 4A). One bundle appears almost perpendicular to the membrane and contacts a single *c* subunit near the middle of the membrane. The other bundle appears tilted and contacts the adjacent *c* subunit closer to the periplasm. This arrangement brings the two *c* subunits in distinct chemical environments and establishes the conditions necessary for a two half-channel model of proton translocation [48].

Whereas subunit *a* has underwent little changes during evolution, subunit *c* has been a large evolutionary playground [82]. A lot of archaea have an 8 kDa *c* subunit with two transmembrane α-helices [35,83–85], but some archaea have very unusual *c* subunits. A 16 kDa *c* subunit with four transmembrane α-helices is present in all species of *Pyrococcus*, *Thermococcus*, *Methanobrevibacter*, *Methanobacterium*, *Desulfurococcus*, *Staphylothermus* and in *Ignisphaera aggregans* [86] as well as in *Methanothermobacter thermautotrophicus* [87] and *Methanosphaera*

stadtmanae [82,88]. *Methanocaldococcus jannaschii* and *Methanococcus maripaludis* have a triplicated *c* subunit (a *c* subunit with three hairpins and six transmembrane helices) with a molecular mass of around 21 kDa [89]. Also *Methanopyrus kandleri* is very special, because it is the only organism known so far, which has a *c* ring consisting of only one *c* subunit with 13 hairpins and therefore 13 ion-binding sites [82,90].

Although the variation in size is already unique, even more important, also for function, is the variation in number of ion binding sites

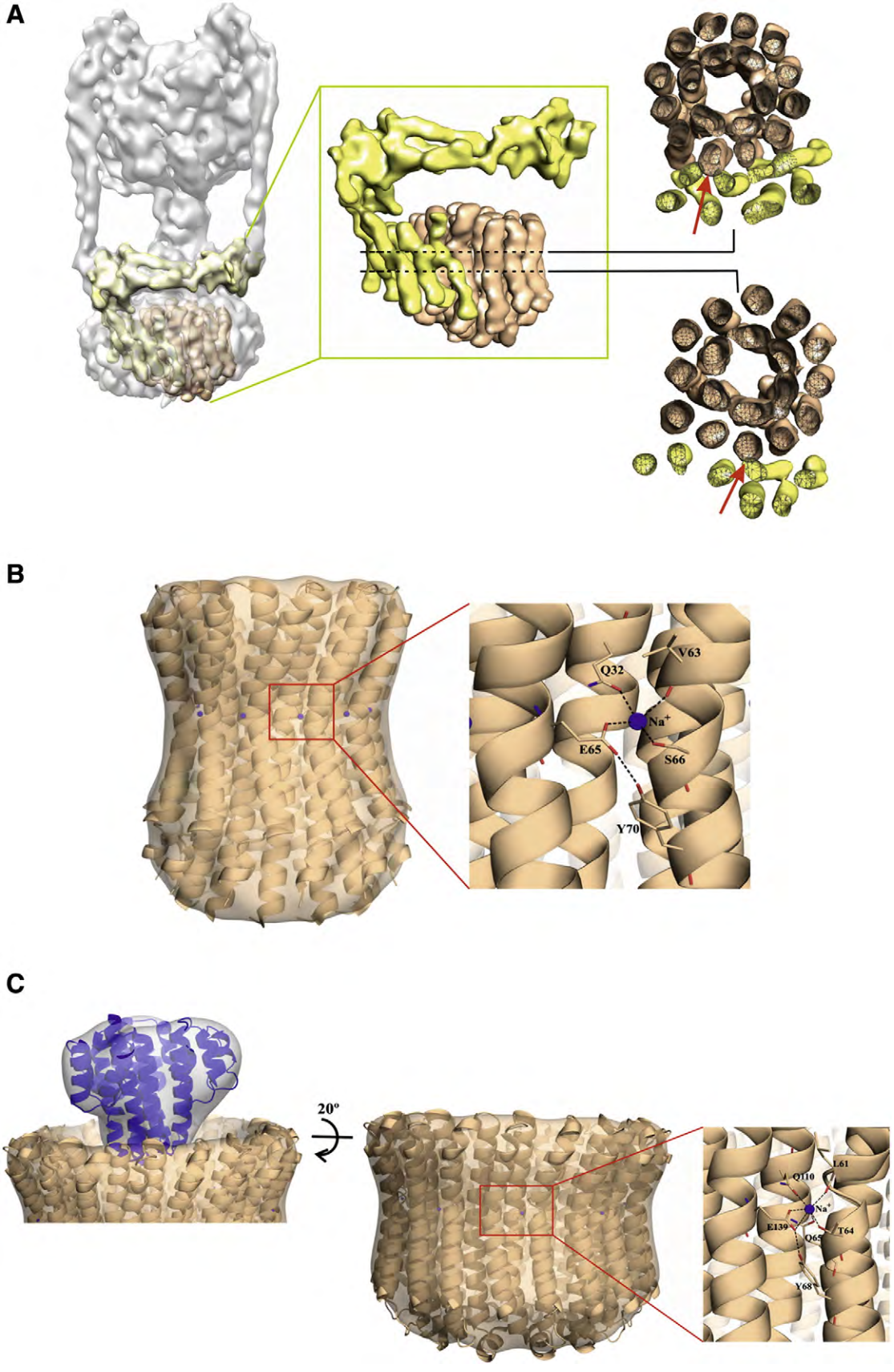

per *c* subunit. In bacterial F_1F_O ATP synthases, the *c* ring is made by multiple copies (10–15) of one subunit [91]. The 16 kDa *c* subunit with four transmembrane α-helices of e.g. Pyrococci and Thermococci lost one ion binding site [86] and the triplicated *c* subunit from *M. jannaschii* [89] and *M. maripaludis* also lost one. This has enormous consequences for the function of the enzyme. If we consider *c* rings to have the same number of transmembrane α-helices, the *c* rings from Pyrococci and Thermococci have only half the number of ion binding sites per ATP synthesizing units. According to:

$$\Delta G_P = -n \times F \times \Delta\tilde{\mu}_{ion} \quad (2)$$

where ΔG_P = phosphorylation potential, n = number of translocated ions, F = Faraday constant, and $\Delta\tilde{\mu}_{ion}$ = electrochemical potential of the coupling ion (Na^+ or H^+), the loss of one ion binding site in every second hairpin of the rotor would lower the number of ions by half. The resulting value for "*n*" (ions/ATP) of two is not enough to generate a phosphorylation potential of ~50 to 70 kJ/mol and thus the enzyme is no longer able to pump ions against this potential and thus unable to synthesize ATP. Since the A_1A_O ATP synthases from Pyrococci and Thermococci are the only ATP synthases encoded in the genome [92], they must synthesize ATP at the expense of $\Delta\tilde{\mu}_{ion}$ *in vivo*. A solution to this enigma is a *c* ring that has more *c* subunits and indeed, circumstantial evidence point to a c_{10} ring in *P. furiosus* [47].

5. Ion translocation and -specificity of the *c* ring of A_1A_O ATP synthases

The *c* ring is the ion carrier and the primary structure of the *c* ring determines which ion binds to the *c* ring. *c* rings from most archaea and bacteria are proton selective and the proton binding site is the conserved carboxylate (Glu, Asp) present in helix two of the 8 kDa *c* subunit [93]. The H^+ is bound between the carboxyl oxygen of the conserved carboxylate and the main chain carbonyl of another amino acid, for example phenylalanine [93]. Very few *c* subunits, notably from anaerobic bacteria and archaea use Na^+ instead of H^+ [94,95]. The Na^+ binding site of e.g. *Ilyobacter tartaricus* contains the before mentioned carboxylate and three more amino acid residues that coordinate the Na^+ [96,97]. These are: Q32, V63 and S66. Y70 forms a hydrogen bond with E65 and stabilizes the geometry of the ion coordination shell, but is not directly involved in Na^+ coordination. T67 itself is also not directly involved in Na^+ binding but coordinates a buried structural water molecule in the Na^+ binding site (Fig. 4B (inset)). Of these residues, only three are adequately conserved to be spotted by sequence comparisons. These are Q32, E65 and S66. Q is substituted and functionally conserved by E, and S by T in some species. Thus the minimal and sufficient motif for Na^+ binding is Q/E…E T/S. This motif is also present in the A_1A_O ATP synthase of some archaea (see below) as well as *E. hirae*. In the A_1A_O ATP synthase *c* ring of *E. hirae* (also called "bacterial V_1V_O ATPase") a similar Na^+ binding site is observed with the essential carboxylate E139 as well as Q110, L61, T64 and Q65, which form the ion coordination shell and Y68 which makes hydrogen bonding interaction with E139 (Fig. 4C (inset)).

As pointed out above, due to the variation in the number of protomers the diameters of these *c* ring rotors differ from organism to organism. A significant structural difference between *c* rings of F_1F_O and A_1A_O ATP synthases is represented by the comparison of the Na^+-translocating undecameric ring of *I. tartaricus c* ring (F_1F_O ATP synthase) and the *c* ring of the *E. hirae* A_1A_O ATP synthase (Fig. 4). Whereas the *I. tartaricus c* ring forms a cylindrical, hourglass shaped protein complex with an outer diameter of ~50 Å and an inner diameter of ~17 Å [98], the decameric ring of *E. hirae* is much more wider spanning an external diameter of 83 Å and an inner diameter of 54 Å [96]. Although among all the solved *c* ring structures, the *E. hirae c* ring has only 10 protomers, the external *c* ring diameter is wider than the one of F_1F_O ATP synthase *c* rings. This structural feature enables the funnel shaped subunit C of A_1A_O ATP synthase, which is not present in F_1F_O ATP synthases, to penetrate into the central cavity of the *c* ring [52], and allowing a direct translation event between *c* ring rotation and ATP synthesis in the A_3B_3 headpiece (Fig. 4B).

A sequence comparison of all the sequences available for *c* subunits (as of Sept. 1., 2013) revealed the Na^+ binding motif Q/E…E T/S to be present in all methanogens and halobacteria, as well as in species of the genera *Pyrococcus*, *Thermococcus*, *Desulfurococcus*, *Ignisphaera*, *Staphylothermus and Nanoarchaeum* (Table 1). Of these, the A_1A_O ATP synthases from *Methanobrevibacter ruminantium* and *P. furiosus* have been shown to be Na^+ specific [65,86,99]. Structural models of a c_{10} ring of *P. furiosus* and a c_3 construct of *M. ruminantium*, generated computationally, revealed the nature of the Na^+ binding sites (Fig. 5) [86]. The c_{10} ring and the c_3 construct consist of *c* subunits with four transmembrane helices each. In the c_{10} ring of *P. furiosus* the Na^+ binding site is within one *c* subunit flanked by transmembrane helix 2 (TM2) and helix 4 (TM4). The Na^+ is coordinated by E142 (TM4), Q113 (TM3), T56 (TM2), and Q57 (TM2), and by the backbone of L53 (TM2). Y60 (TM2) is not directly involved in Na^+ coordination, but forms a hydrogen-bond with E142, and therefore stabilizes the geometry of the ion-coordination shell (Fig. 5A). This kind of network is identical to that revealed by the crystal structure of the c_{10} rotor from *E. hirae* [96]. Between two *c* subunits is no second ion binding site in the *c* ring of *P. furiosus* (Fig. 5B). There the essential glutamate of the Na^+ binding site was replaced by a methionine (M55) during evolution and therefore nature designed an unusual *c* ring with only one Na^+ binding site in one *c* subunit. This is different in the *c* ring of *M. ruminantium*. As was evident from sequence comparisons and confirmed by modeling studies using a c_3 construct, *M. ruminantium* has one Na^+ binding site within one *c* subunit (Fig. 5C), as in *P. furiosus*, but also a second Na^+ binding site between two *c* subunits (Fig. 5D). Both Na^+ binding sites are completely identical in their amino acid composition. Within one *c* subunit the Na^+ is coordinated by the side chains of the amino acids E140 (TM4), Q111 (TM3), Q61 (TM2) T60 (TM2) and L57 (TM2). Again Y64 (TM2) is for hydrogen-bonding with the side chain of E140. The second Na^+ binding site in the *c* ring of *M. ruminantium* is between two *c* subunits. Again E59 (TM2′), Q30 (TM1′), Q142 (TM4), T141 (TM4) and L138 (TM4) are directly involved in Na^+ coordination. Y145 (TM4) stabilizes the geometry of the ion-coordination shell by hydrogen-bonding with E59 [86]. Therefore nature designed in the case of *M. ruminantium* a *c* ring, which has one Na^+ binding site within and another between each *c* subunit.

6. Adaptations of archaeal ATP synthases to the inhospitable environments their hosts thrive in

Sodium bioenergetics is advantageous for organisms that live on the thermodynamic edge of life [20] like methanogens or *T. onnurineus* thriving on formate. Any reduction in the magnitude of the electrochemical ion potential across the membrane by leakage of ions back into the cell would be detrimental. Biological membranes are leakier for protons than for sodium ions [102]. Thus, a sodium bioenergetics is

Fig. 4. (A) The three-dimensional EM map of the *T. thermophilus* enzyme at 9.7 Å resolution (EM Database ID: EMD 5335 [48]) is shown as gray surface. The density corresponding to the *c* ring (wheat) and subunit *a* (yellow) are shown as solid surface. Two cross-sections of the map segments near the middle of the *c*-ring show the contacts of *c* subunits with helices of the *a* subunit at two positions (indicated by red arrows). (B) Structure of the *c* ring of the F_1F_O ATP synthase from *Ilyobacter tartaricus* (PDB ID: 1YCE [98]) showing a narrower cylindrical, hourglass shaped complex. (inset) Sodium ion binding site with the ion coordination shell formed by E65, Q32, V63 and S66 and Y70 is making a hydrogen bond with E65 to stabilize the geometry. (C) The A_1A_O ATP synthase *c* ring structure from *E. hirae* (PDB ID: 2BL2 [96]) revealing a wider diameter at the upper part of the cylinder, which could accommodate the funnel shaped C subunit (left; PDB ID: 1R5Z [51]; blue). (inset) Sodium ion binding site of the *E. hirae c* ring showing the Na^+ coordination shell formed by amino acids E139, Q110, L61, T64 and Q65 and Y68 having hydrogen bonding interaction with E139.

seen as the primary event in the evolution of bioenergetics [20,103,104]. Indeed, an acetogen with an ancient pathway in which carbon dioxide fixation is coupled to ATP synthesis by a chemiosmotic mechanism relies on a sodium potential. This pathway allows for the synthesis of only a fraction of an ATP [104]. The same is true for methanogens that employ pretty much the same pathway [29]. So far, sodium bioenergetics has

Table 1
Ion binding motifs of different archaeal and bacterial *c* subunits.

Organism		Site 1[b]	Site 2[b]	Ion[c]
Bacteria (*c* subunits with one hairpin)[d]				
Acetobacterium woodii c_2/c_3		Q	VxETTxxY	Na^+ •
Ilyobacter tartaricus		Q	VxESTxxY	Na^+ •
Propionigenium modestum		Q	IxESTxxY	Na^+ •
Bacillus subtilis		N	LxEALxxI	H^+ •
Escherichia coli		I	LxDAIxxI	H^+ •
Bacteria (*c* subunits with two hairpins)				
Enterococcus hirae[e]	[a]H1-H2	V	LxGTQxxY	--
	H3-H4	Q	MxETYxxL	Na^+ •
Euryarchaeota (*c* subunits with one hairpin)[f]				
Archaeoglobus fulgidus		E	IxETIxxF	Na^+
Ferroglobus placidus		E	IxETIxxF	Na^+
Haladaptatus paucihalophilus		E	LxETLxxL	Na^+
Halalkalicoccus jeotgali		E	LxETLxxL	Na^+
Haloarcula hispanica		E	LxETLxxL	Na^+
Halobacterium salinarum		E	LxETLxxL	Na^+
Haloferax volcanii		E	LxETLxxL	Na^+
Halogeometricum borinquense		E	LxETLxxL	Na^+
Halopiger xanaduensis		E	LxETLxxL	Na^+
Haloquadratum walsbyi		E	LxETIxxL	Na^+
Halorhabdus utahensis		E	LxETLxxL	Na^+
Halorubrum lacusprofundi		E	LxETIxxL	Na^+
Haloterrigena turkmenica		E	LxETLxxL	Na^+
Methanocella paludicola		Q	IxETLxxL	Na^+
Methanococcoides burtonii		E	IxETIxxF	Na^+
Methanocorpusculum labreanum		E	LxETVxxF	Na^+
Methanoculleus marisnigri		E	IxETIxxF	Na^+
Methanohalobium evestigatum		E	IxETIxxF	Na^+
Methanohalophilus mahii		E	IxETIxxF	Na^+
Methanomethylovorans hollandica		E	IxETIxxF	Na^+
Methanoplanus petrolearius		Q	IxETVxxF	Na^+
Methanoregula boonei		E	IxETIxxF	Na^+
Methanosaeta concilii		E	LxETLxxF	Na^+
Methanosalsum zhilinae		Q	IxEAIxxF	H^+
Methanosarcina acetivorans		E	IxETIxxF	Na^+/H^+ •
Methanosphaerula palustris		E	IxETIxxF	Na^+
Methanothermus fervidus		Q	LxETHxxF	Na^+
Natrialba magadii		E	LxETLxxL	Na^+
Natronococcus occultus		E	LxETLxxF	Na^+
Natronomonas pharaonis		E	LxETLxxL	Na^+
Natronorubrum tibetense		E	LxETLxxL	Na^+
Picrophilus torridus		Q	IxETLxxI	Na^+
Thermoplasma acidophilum		Q	IxETLxxI	Na^+
Euryarchaeota (*c* subunits with two hairpins)				
Methanobacterium sp. AL-21[g]	[a]H1-H2	Q	LxETQxxY	Na^+
	H3-H4	Q	LxETQxxY	Na^+
Methanobrevibacter ruminantium[g]	H1-H2	Q	LxETQxxY	Na^+ •
	H3-H4	Q	LxETQxxY	Na^+ •
Methanosphaera stadtmanae[g]	H1-H2	Q	IxETQxxY	Na^+
	H3-H4	Q	IxETQxxY	Na^+
Methanothermobacter thermautotrophicus[g]	H1-H2	Q	LxETQxxY	Na^+
	H3-H4	Q	LxETQxxY	Na^+
Pyrococcus furiosus[e]	H1-H2	V	LxMTQxxY	--
	H3-H4	Q	MxETMxxF	Na^+ •
Thermococcus onnurineus[e]	H1-H2	V	LxMTQxxY	--
	H3-H4	Q	MxETMxxF	Na^+

(continued on next page)

Table 1 (*continued*)

Organism		Site 1[b]	Site 2[b]	Ion[c]
Euryarchaeota (*c* subunits with three hairpins)[h]				
Methanocaldococcus jannaschii	[a]H1-H2	A	LxQTQxxY	--
	H3-H4	Q	LxETQxxY	Na^+
	H5-H6	Q	MxETFxxF	Na^+
Methanococcus maripaludis	H1-H2	A	LxQTQxxY	--
	H3-H4	Q	LxETQxxY	Na^+
	H5-H6	Q	MxETFxxF	Na^+
Methanospirillum hungatei	H1-H2	V	IxQTQxxY	--
	H3-H4	Q	VxETQxxY	Na^+
	H5-H6	Q	MxETFxxF	Na^+
Methanothermococcus okinawensis	H1-H2	A	LxQTQxxY	--
	H3-H4	Q	LxETQxxY	Na^+
	H5-H6	Q	MxETFxxF	Na^+
Methanotorris igneus	H1-H2	A	LxQTQxxY	--
	H3-H4	Q	LxETQxxY	Na^+
	H5-H6	Q	MxETFxxF	Na^+
Euryarchaeota (*c* subunits with 13 hairpins)				
Methanopyrus kandleri[i]		Q	FxETQxxY	Na^+
Crenarchaeota (*c* subunits with one hairpin)[f]				
Acidianus hospitalis		V	IxEGIxxY	H^+
Acidilobus saccharovorans		V	LxEGIxxY	H^+
Aeropyrum pernix		V	LxEGIxxY	H^+
Caldisphaera lagunensis		V	LxEGIxxY	H^+
Caldivirga maquilingensis		M	FxETIxxY	H^+
Hyperthermus butylicus		L	LxEGIxxY	H^+
Ignicoccus hospitalis		L	IxETPxxY	H^+
Metallosphaera sedula		V	IxEGIxxY	H^+
Pyrobaculum aerophilum		V	LxEAIxxY	H^+
Pyrolobus fumarii		V	LxEGIxxY	H^+
Sulfolobus acidocaldarius		V	IxEGIxxY	H^+
Thermofilum pendens		L	LxEGIxxY	H^+
Thermoproteus neutrophilus		L	LxEAVxxY	H^+
Thermosphaera aggregans		Q	YxELWxxL	H^+
Vulcanisaeta distributa		I	LxEAIxxY	H^+
Crenarchaeota (*c* subunits with two hairpins)[g]				
Desulfurococcus kamchatkensis	[a]H1-H2	M	LxMTQxxY	--
	H3-H4	Q	YxELWxxY	Na^+
Ignisphaera aggregans	H1-H2	T	FxMTQxxA	--
	H3-H4	Q	YxELFxxI	Na^+
Staphylothermus marinus	H1-H2	M	LxMTQxxY	--
	H3-H4	Q	YxELIxxL	Na^+
Nanoarchaeota (*c* subunits with one hairpin)[f]				
Nanoarchaeum equitans		Q	LxETQxxY	Na^+
Korarchaeota (*c* subunits with one hairpin)[f]				
Korarchaeum cryptofilum		L	LxEGVxxY	H^+
Thaumarchaeota (*c* subunits with one hairpin)[f]				
Cenarchaeum symbiosum		L	MxESIxxY	H^+
Nitrosopumilus maritimus		L	MxESIxxY	H^+
Nitrosoarchaeum limnia		L	MxESIxxY	H^+
Nitrososphaera gargensis		L	MxESIxxY	H^+

[a] H1 = Helix 1, H2 = Helix 2, H3 = Helix 3, H4 = Helix 4, H5 = Helix 5, H6 = Helix 6.
[b] Site 1 and 2 describes amino acids of the H^+ or Na^+ binding motif in helix one and two of the hairpin-like c subunit.
[c] Except were indicated (●, experimental evidence), the ion specificity is suggested based on the presence or absence of the Na^+ binding motif.
[d] In bacterial c subunits, the ion binding site is between two c subunits and built by Q (site 1) and ET (site 2).
[e] In these c subunits, the Na^+ binding motif is shared by H1–H2 and H3–H4. There is only one Na^+ binding site in four transmembrane helices.
[f] As in bacterial c subunits, the ion binding site is between two c subunits and built by Q (site 1) and ET (site 2).
[g] These c subunits have two ion binding sites in four transmembrane helices. One is within one c subunit, one inbetween two c subunits.
[h] In these c subunits, the Na^+ binding motif is shared by H1–H2, H3–H4 and H5–H6. There are two Na^+ binding sites in six transmembrane helices.
[i] This c subunit has thirteen covalently linked hairpins, each has the depicted Na^+ binding site.

only been observed in anaerobes. In addition to living in low energy environments these environments are full of fermentation end products such as short chain fatty acids. These act as proton ferries to decouple metabolism from ATP synthesis. These fermentation end products cannot shuffle back Na^+ into the cell and thus, a Na^+ potential is not dissipated by short chain fatty acids [20].

A Na^+-dependent A_1A_O ATP synthase is fully consistent with the physiology of *M. ruminantium*. It has no cytochromes and only the Na^+-

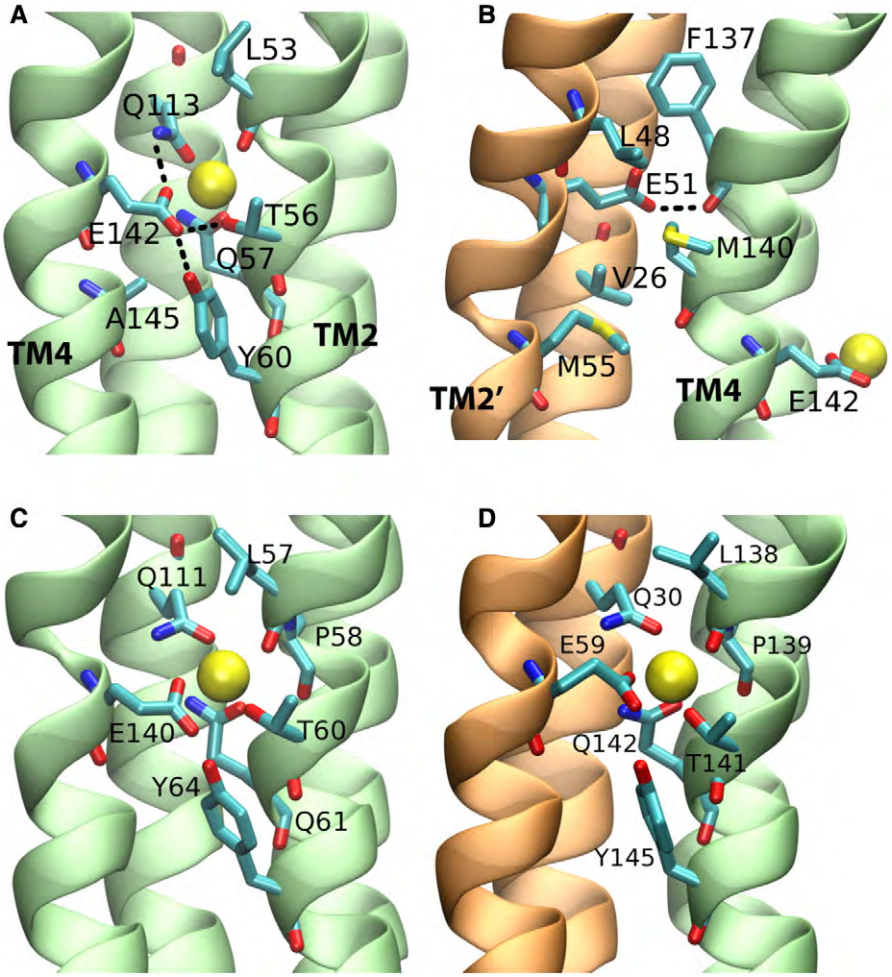

Fig. 5. (A) Computationally derived structural model of the Na^+ binding site of the *c* ring from *P. furiosus*. The ion binding site is within one *c* subunit between TM2 and TM4. The Na^+ is coordinated by E142 (TM4), Q113 (TM3), T56 (TM2), and Q57 (TM2), and by the backbone of L53 (TM2). Y60 (TM2) is not directly involved in Na^+ coordination, but forms a hydrogen-bond with E142. (B) Between two *c* subunits is no second ion binding site in the *c* ring of *P. furiosus*. There the essential glutamate of the Na^+ binding site is replaced by a methionine (M55). (C) The *c* ring of *M. ruminantium* has two Na^+ binding sites. According to the computationally derived model [86] the Na^+ is coordinated by the side chains of the amino acids E140 (TM4), Q111 (TM3), Q61 (TM2) T60 (TM2) and L57 (TM2) within one *c* subunit. Again Y64 (TM2) is for hydrogen-bonding with the side chain of E140. (D) The second Na^+ binding site in *M. ruminantium* is between two *c* subunits. Again E59 (TM2′), Q30 (TM1′), Q142 (TM4), T141 (TM4) and L138 (TM4) are directly involved in Na^+ coordination. Y145 (TM4) stabilizes the geometry of the ion-coordination shell by hydrogen-bonding with E59 [86].

motive methyltransferase for membrane energization and thus, the Na^+ potential must be used to drive ATP synthesis [20,29,86]. With the evolution of cytochromes and an additional proton-pumping electron transfer chain in some methanogens like the *Methanosarcinales*, an organism arose that couples its metabolism to the generation of a proton potential and a sodium ion potential. The ATP synthase adapted to this scenario by using Na^+ and H^+ [29,30]. Apparently, Na^+ and H^+ concurrently drive ATP synthesis. The ion binding site has a high preference for H^+, but under physiological conditions of pH 7.5 and 400 mM NaCl (sea water) both Na^+ and H^+ are used simultaneously [100]. The minimal Na^+ binding motif is conserved but the residues involved in Na^+ binding in bacterial *c* subunits are less conserved. Noteworthy is the change of glutamine (Q) of the sodium binding motif Q…ES/T to a second glutamate, and indeed, this exchange still allows for Na^+ binding [101]. Such a Q → E exchange is present in a lot of methanogens (Table 1).

The ion specificity of the membrane-bound hydrogenase (Mbh) of *P. furiosus* has not been addressed experimentally, but there is no reason to believe that sodium ions are not the coupling ion. It is also noteworthy, that some of the halophilic archaea have a sodium ion binding site: but whether the ATP synthase indeed uses Na^+ or Na^+ and H^+ has to be established. Apart from the *Euryarchaeota* (Methanogens, Thermococci and Pyrococci), only the genera *Desulfurococcus*, *Ignisphaera* and *Staphylothermus* of the phylum *Crenarchaeota* [86] as well as *Nanoarchaeum equitans* of the phylum *Nanoarchaeota* have the conserved Na^+ binding site. Unfortunately, nothing is known about their physiology but it can be concluded that Na^+ is important for their physiology.

Another adaptation is the increase in length of the *c* subunits with increasing temperature. At least in methanogens, there is a clear tendency from one hairpin (most methanogens, e. g. *M. mazei*, 35 °C) to two hairpins (*M. thermautotrophicus*, 70 °C), three hairpins (*M. jannaschii*, 85 °C) and 13 hairpins (*M. kandleri*, 98 °C). The higher the number of covalent linkages the higher the stability of the rotating *c* ring. These arguments may be true for the two peripheral stalks that may gives additional stability to the rotating nanomachine.

7. Conclusion

A_1A_O ATP synthases of hyperthermophilic archaea have unique structural and functional features, including an optimized P-loop design of the catalytic A subunit, enabling the enzyme to catalyze ATP apart from GTP and UTP. The 80 Å long central stalk with its subunits C, D and F, reflects a coupling mechanism diverse to the Wankel engine like form, described for the γ–ε stalk ensemble of F_1F_O ATP synthase. A hallmark of the classification of A_1A_O ATP synthases is the number

and structures of peripheral stalk subunits (E–H). A primary function is to allow the rotary elements of A_O and A_1 to move relative to each other. Their importance for regulation and fine-tuning of the entire enzyme will be a topic for the near future. So far, biochemical and structural work on these unique enzymes has been done with enzymes isolated directly from cells of these hyperthermophiles. Since these are difficult to grow and yields are low, biochemical analyses are a challenge and not possible for many interesting archaea. The advent of genetic systems, overexpression, tagging and affinity purification will bring the field into the next round. There is still lot to do to unravel the beauty of these fascinating enzymes.

Acknowledgments

This work was supported by a grant from the Deutsche Forschungsgemeinschaft (through SFB 807, V. Müller) and the Ministry of Education-Singapore (MOE) (MOE2011-T2-2-156; ARC 18/12; G. Grüber).

References

[1] K.O. Stetter, History of discovery of the first hyperthermophiles, Extremophiles 10 (2006) 357–362.
[2] G. Fiala, K.O. Stetter, *Pyrococcus furiosus* sp. nov. represents a novel genus of marine heterotrophic archaebacteria growing optimally at 100 °C, Arch. Microbiol. 145 (1986) 56–61.
[3] K.O. Stetter, H. König, E. Stackebrandt, *Pyrodictium* gen. nov., a new genus of submarine disc-shaped sulphur reducing archaebacteria growing optimally at 105 °C, Syst. Appl. Microbiol. 4 (1983) 535–551.
[4] W. Zillig, I. Holz, D. Janekovic, H.P. Klenk, E. Imsel, J. Trent, S. Wunderl, V.H. Forjaz, R. Coutinho, T. Ferreira, *Hyperthermus butylicus*, a hyperthermophilic sulfur-reducing archaebacterium that ferments peptides, J. Bacteriol. 172 (1990) 3959–3965.
[5] M. Kurr, R. Huber, H. Konig, H.W. Jannasch, H. Fricke, A. Trincone, J.K. Kristjansson, K.O. Stetter, *Methanopyrus kandleri*, gen. and sp. nov. represents a novel group of hyperthermophilic methanogens, growing at 110 °C, Arch. Microbiol. 156 (1991) 239–247.
[6] E. Blöchl, R. Rachel, S. Burggraf, D. Hafenbradl, H.W. Jannasch, K.O. Stetter, *Pyrolobus fumarii*, gen. and sp. nov., represents a novel group of archaea, extending the upper temperature limit for life to 113 °C, Extremophiles 1 (1997) 14–21.
[7] H.P. Klenk, M. Spitzer, T. Ochsenreiter, G. Fuellen, Phylogenomics of hyperthermophilic *Archaea* and *Bacteria*, Biochem. Soc. Trans. 32 (2004) 175–178.
[8] B. Snel, M.A. Huynen, B.E. Dutilh, Genome trees and the nature of genome evolution, Annu. Rev. Microbiol. 59 (2005) 191–209.
[9] S. Gribaldo, C. Brochier-Armanet, The origin and evolution of *Archaea*: a state of the art, Philos. Trans. R. Soc. Lond. B Biol. Sci. 361 (2006) 1007–1022.
[10] D.W. Schwartzman, C.H. Lineweaver, The hyperthermophilic origin of life revisited, Biochem. Soc. Trans. 32 (2004) 168–171.
[11] T.M. Hoehler, Biogeochemistry of dihydrogen (H_2), Met. Ions Biol. Syst. 43 (2005) 9–48.
[12] J.P. Amend, E.L. Shock, Energetics of overall metabolic reactions of thermophilic and hyperthermophilic archaea and bacteria, FEMS Microbiol. Rev. 25 (2001) 175–243.
[13] R. Conrad, Soil microorganisms as controllers of atmospheric trace gases (H_2, CO, CH_4, OCS, N_2O, and NO), Microbiol. Rev. 60 (1996) 609–640.
[14] H. Elderfield, A. Schultz, Mid-ocean ridge hydrothermal fluxes and the chemical composition of the ocean, Annu. Rev. Earth Planet. Sci. 24 (1996) 191–224.
[15] D.S. Kelley, J.A. Baross, J.R. Delaney, Volcanoes, fluids, and life at mid-ocean ridge spreading centers, Annu. Rev. Earth Planet. Sci. 30 (2002) 385–491.
[16] T.M. McCollom, J.S. Seewald, Abiotic synthesis of organic compounds in deep-sea hydrothermal environments, Chem. Rev. 107 (2007) 382–401.
[17] U. Deppenmeier, V. Müller, Life close to the thermodynamic limit: how methanogenic archaea conserve energy, Results Probl. Cell Differ. 45 (2008) 123–152.
[18] E.J. Boekema, J.F. van Breemen, A. Brisson, T. Ubbink-Kok, W.N. Konings, J.S. Lolkema, Connecting stalks in V-type ATPase, Nature 401 (1999) 37–38.
[19] G. Schäfer, M. Engelhard, V. Müller, Bioenergetics of the *Archaea*, Microbiol. Mol. Biol. Rev. 63 (1999) 570–620.
[20] F. Mayer, V. Müller, Adaptations of anaerobic archaea to life under extreme energy limitation, FEMS Microbiol. Rev. (2013), http://dx.doi.org/10.1111/1574-6976.12043.
[21] R. Sapra, K. Bagramyan, M.W.W. Adams, A simple energy-conserving system: proton reduction coupled to proton translocation, Proc. Natl. Acad. Sci. U. S. A. 100 (2003) 7545–7550.
[22] G.J. Schut, E.S. Boyd, J.W. Peters, M.W. Adams, The modular respiratory complexes involved in hydrogen and sulfur metabolism by heterotrophic hyperthermophilic archaea and their evolutionary implications, FEMS Microbiol. Rev. 37 (2012) 182–203.
[23] Y.J. Kim, H.S. Lee, E.S. Kim, S.S. Bae, J.K. Lim, R. Matsumi, A.V. Lebedinsky, T.G. Sokolova, D.A. Kozhevnikova, S.S. Cha, S.J. Kim, K.K. Kwon, T. Imanaka, H. Atomi, E.A. Bonch-Osmolovskaya, J.H. Lee, S.G. Kang, Formate-driven growth coupled with H_2 production, Nature 467 (2010) 352–355.
[24] J.K. Lim, S.S. Bae, T.W. Kim, J.H. Lee, H.S. Lee, S.G. Kang, Thermodynamics of formate-oxidizing metabolism and implications for H_2 production, Appl. Environ. Microbiol. 78 (2012) 7393–7397.
[25] U. Deppenmeier, The unique biochemistry of methanogenesis, Prog. Nucleic Acid Res. Mol. Biol. 71 (2002) 223–283.
[26] V. Müller, C. Winner, G. Gottschalk, Electron transport-driven sodium extrusion during methanogenesis from formaldehyde + H_2 by *Methanosarcina barkeri*, Eur. J. Biochem. 178 (1988) 519–525.
[27] G. Gottschalk, R.K. Thauer, The Na^+-translocating methyltransferase complex from methanogenic archaea, Biochim. Biophys. Acta 1505 (2001) 28–36.
[28] U. Deppenmeier, Redox-driven proton translocation in methanogenic archaea, Cell. Mol. Life Sci. 59 (2002) 1–21.
[29] R.K. Thauer, A.K. Kaster, H. Seedorf, W. Buckel, R. Hedderich, Methanogenic archaea: ecologically relevant differences in energy conservation, Nat. Rev. Microbiol. 6 (2008) 579–591.
[30] K. Schlegel, V. Müller, Evolution of Na^+ and H^+ bioenergetics in methanogenic archaea, Biochem. Soc. Trans. 41 (2013) 421–426.
[31] V. Müller, C. Ruppert, T. Lemker, Structure and function of the A_1A_O ATPases from methanogenic archaea, J. Bioenerg. Biomembr. 31 (1999) 15–28.
[32] V. Müller, G. Grüber, ATP synthases: structure, function and evolution of unique energy converters, Cell. Mol. Life Sci. 60 (2003) 474–494.
[33] K.Y. Pisa, C. Weidner, H. Maischak, H. Kavermann, V. Müller, The coupling ion in methanoarchaeal ATP synthases: H^+ versus Na^+ in the A_1A_O ATP synthase from the archaeon *Methanosarcina mazei* Gö1, FEMS Microbiol. Lett. 277 (2007) 56–63.
[34] K. Lewalter, V. Müller, Bioenergetics of archaea: ancient energy conserving mechanisms developed in the early history of life, Biochim. Biophys. Acta 1757 (2006) 437–445.
[35] R. Wilms, C. Freiberg, E. Wegerle, I. Meier, F. Mayer, V. Müller, Subunit structure and organization of the genes of the A_1A_O ATPase from the archaeon *Methanosarcina mazei* Gö1, J. Biol. Chem. 271 (1996) 18843–18852.
[36] A. Lingl, H. Huber, K.O. Stetter, F. Mayer, J. Kellermann, V. Müller, Isolation of a complete A_1A_O ATP synthase comprising nine subunits from the hyperthermophile *Methanococcus jannaschii*, Extremophiles 7 (2003) 249–257.
[37] R.L. Cross, L. Taiz, Gene duplication as a means for altering H^+/ATP ratios during the evolution of F_OF_1 ATPases and synthases, FEBS Lett. 259 (1990) 22227–22229.
[38] N. Nelson, The vacuolar H^+-ATPase — one of the most fundamental ion pumps in nature, J. Exp. Biol. 172 (1992) 19–27.
[39] R.L. Cross, V. Müller, The evolution of A-, F-, and V-type ATP synthases and ATPases: reversals in function and changes in the H^+/ATP stoichiometry, FEBS Lett. 576 (2004) 1–4.
[40] G. Grüber, H. Wieczorek, W.R. Harvey, V. Müller, Structure–function relationships of A-, F- and V-ATPases, J. Exp. Biol. 204 (2001) 2597–2605.
[41] E. Hilario, J.P. Gogarten, The prokaryote-to-eukaryote transition reflected in the evolution of the V/F/A-ATPase catalytic and proteolipid subunits, J. Mol. Evol. 46 (1998) 703–715.
[42] Y. Mukohata, K. Ihara, Situation of archaebacterial ATPase among ion-translocating ATPase, in: C.H. Kim, T. Ozawa (Eds.), Bioenergetics, Plenum Press, New York, 1990, pp. 205–216.
[43] G. Schäfer, M. Meyering-Vos, F-type or V-type? The chimeric nature of the archaebacterial ATP synthase, Biochim. Biophys. Acta 1101 (1992) 232–235.
[44] T. Ubbink-Kok, E.J. Boekema, J.F. van Breemen, A. Brisson, W.N. Konings, J.S. Lolkema, Stator structure and subunit composition of the V_1V_O Na^+-ATPase of the thermophilic bacterium *Caloramator fervidus*, J. Mol. Biol. 296 (2000) 311–321.
[45] Ü. Coskun, Y.L. Chaban, A. Lingl, V. Müller, W. Keegstra, E.J. Boekema, G. Grüber, Structure and subunit arrangement of the A-type ATP synthase complex from the archaeon *Methanococcus jannaschii* visualized by electron microscopy, J. Biol. Chem. 279 (2004) 38644–38648.
[46] R.A. Bernal, D. Stock, Three-dimensional structure of the intact *Thermus thermophilus* H^+-ATPase/synthase by electron microscopy, Structure 12 (2004) 1789–1798.
[47] J. Vonck, K.Y. Pisa, N. Morgner, B. Brutschy, V. Müller, Three-dimensional structure of A_1A_O ATP synthase from the hyperthermophilic archaeon *Pyrococcus furiosus* by electron microscopy, J. Biol. Chem. 284 (2009) 10110–10119.
[48] W.C. Lau, J.L. Rubinstein, Subnanometre-resolution structure of the intact *Thermus thermophilus* H^+-driven ATP synthase, Nature 481 (2012) 214–218.
[49] A. Kumar, M.S. Manimekalai, A.M. Balakrishna, J. Jeyakanthan, G. Grüber, Nucleotide binding states of subunit A of the A-ATP synthase and the implication of P-loop switch in evolution, J. Mol. Biol. 396 (2010) 301–320.
[50] I.B. Schäfer, S.M. Bailer, M.G. Düser, M. Börsch, R.A. Bernal, D. Stock, G. Grüber, Crystal structure of the archaeal A_1A_O ATP synthase subunit B from *Methanosarcina mazei* Gö1: implications of nucleotide-binding differences in the major A_1A_O subunits A and B, J. Mol. Biol. 358 (2006) 725–740.
[51] M. Iwata, H. Imamura, E. Stambouli, C. Ikeda, M. Tamakoshi, K. Nagata, H. Makyio, B. Hankamer, J. Barber, M. Yoshida, K. Yokoyama, S. Iwata, Crystal structure of a central stalk subunit C and reversible association/dissociation of vacuole-type ATPase, Proc. Natl. Acad. Sci. U. S. A. 101 (2004) 59–64.
[52] S. Saijo, S. Arai, K.M. Hossain, I. Yamato, K. Suzuki, Y. Kakinuma, Y. Ishizuka-Katsura, N. Ohsawa, T. Terada, M. Shirouzu, S. Yokoyama, S. Iwata, T. Murata, Crystal structure of the central axis DF complex of the prokaryotic V-ATPase, Proc. Natl. Acad. Sci. U. S. A. 108 (2011) 19955–19960.
[53] S. Gayen, S. Vivekanandan, G. Biukovic, G. Grüber, H.S. Yoon, NMR solution structure of subunit F of the methanogenic A_1A_O adenosine triphosphate synthase

and its interaction with the nucleotide-binding subunit B, Biochemistry 46 (2007) 11684–11694.
[54] M.J. Maher, S. Akimoto, M. Iwata, K. Nagata, Y. Hori, M. Yoshida, S. Yokoyama, S. Iwata, K. Yokoyama, Crystal structure of A_3B_3 complex of V-ATPase from *Thermus thermophilus*, EMBO J. 28 (2009) 3771–3779.
[55] S. Arai, S. Saijo, K. Suzuki, K. Mizutani, Y. Kakinuma, Y. Ishizuka-Katsura, N. Ohsawa, T. Terada, M. Shirouzu, S. Yokoyama, S. Iwata, I. Yamato, T. Murata, Rotation mechanism of *Enterococcus hirae* V_1-ATPase based on asymmetric crystal structures, Nature 493 (2013) 703–707.
[56] Ü. Coskun, M. Radermacher, V. Müller, T. Ruiz, G. Grüber, Three-dimensional organization of the archaeal A_1-ATPase from *Methanosarcina mazei* Gö1, J. Biol. Chem. 279 (2004) 22759–22764.
[57] G. Grüber, D.I. Svergun, Ü. Coskun, T. Lemker, M.H. Koch, H. Schägger, V. Müller, Structural insights into the A_1 ATPase from the archaeon, *Methanosarcina mazei* Gö1, Biochemistry 40 (2001) 1890–1896.
[58] Ü. Coskun, G. Grüber, M.H. Koch, J. Godovac-Zimmermann, T. Lemker, V. Müller, Cross-talk in the A_1-ATPase from *Methanosarcina mazei* Gö1 due to nucleotide-binding, J. Biol. Chem. 277 (2002) 17327–17333.
[59] I. Schäfer, M. Rössle, G. Biukovic, V. Müller, G. Grüber, Structural and functional analysis of the coupling subunit F in solution and topological arrangement of the stalk domains of the methanogenic A_1A_O ATP synthase, J. Bioenerg. Biomembr. 38 (2006) 83–92.
[60] J.P. Abrahams, A.G.W. Leslie, R. Lutter, J.E. Walker, Structure at 2.8 Å resolution of F_1-ATPase from bovine heart mitochondria, Nature 370 (1994) 621–628.
[61] S. Wilkens, Structure of the vacuolar adenosine triphosphatases, Cell Biochem. Biophys. 34 (2001) 191–208.
[62] M. Radermacher, T. Ruiz, H. Wieczorek, G. Grüber, The structure of the V_1-ATPase determined by three-dimensional electron microscopy of single particles, J. Struct. Biol. 135 (2001) 26–37.
[63] L.S. Holliday, M. Lu, B.S. Lee, R.D. Nelson, S. Solivan, L. Zhang, S.L. Gluck, The amino-terminal domain of the B subunit of vacuolar H^+-ATPase contains a filamentous actin binding site, J. Biol. Chem. 275 (2000) 32331–32337.
[64] M.S. Manimekalai, A. Kumar, J. Jeyakanthan, G. Grüber, The transition-like state and P_i entrance into the catalytic A subunit of the biological engine A-ATP synthase, J. Mol. Biol. 408 (2011) 736–754.
[65] K.Y. Pisa, H. Huber, M. Thomm, V. Müller, A sodium ion-dependent A_1A_O ATP synthase from the hyperthermophilic archaeon *Pyrococcus furiosus*, FEBS J. 274 (2007) 3928–3938.
[66] C. Chen, A.K. Saxena, W.N. Simcoke, D.N. Garboczi, P.L. Pedersen, Y.H. Ko, Mitochondrial ATP synthase. Crystal structure of the catalytic F_1 unit in a vanadate-induced transition-like state and implications for mechanism, J. Biol. Chem. 281 (2006) 13777–13783.
[67] C.A. Smith, I. Rayment, X-ray structure of the magnesium(II)-ADP-vanadate complex of the *Dictyostelium discoideum* myosin motor domain to 1.9 Å resolution, Biochemistry 35 (1996) 5404–5417.
[68] A. Kumar, M.S. Manimekalai, A.M. Balakrishna, C. Hunke, S. Weigelt, N. Sewald, G. Grüber, Spectroscopic and crystallographic studies of the mutant R416W give insight into the nucleotide binding traits of subunit B of the A_1A_O ATP synthase, Proteins 75 (2009) 807–819.
[69] R. Watanabe, R. Iino, H. Noji, Phosphate release in F_1-ATPase catalytic cycle follows ADP release, Nat. Chem. Biol. 6 (2010) 814–820.
[70] A. Kumar, M.S. Manimekalai, G. Grüber, Structure of the nucleotide-binding subunit B of the energy producer A_1A_O ATP synthase in complex with adenosine diphosphate, Acta Crystallogr. D Biol. Crystallogr. 64 (2008) 1110–1115.
[71] M.S. Manimekalai, A. Kumar, A.M. Balakrishna, G. Grüber, A second transient position of ATP on its trail to the nucleotide-binding site of subunit B of the motor protein A_1A_O ATP synthase, J. Struct. Biol. 166 (2009) 38–45.
[72] J.P. Abrahams, S.K. Buchanan, M.J. Vanraaij, I.M. Fearnley, A.G.W. Leslie, J.E. Walker, The structure of bovine F_1-ATPase complexed with the peptide antibiotic efrapeptin, Proc. Natl. Acad. Sci. U. S. A. 93 (1996) 9420–9424.
[73] T. Ibuki, K. Imada, T. Minamino, T. Kato, T. Miyata, K. Namba, Common architecture of the flagellar type III protein export apparatus and F- and V-type ATPases, Nat. Struct. Mol. Biol. 18 (2011) 277–282.
[74] Y. Minagawa, H. Ueno, M. Hara, Y. Ishizuka-Katsura, N. Ohsawa, T. Terada, M. Shirouzu, S. Yokoyama, I. Yamato, E. Muneyuki, H. Noji, T. Murata, R. Iino, Basic properties of rotary dynamics of the molecular motor *Enterococcus hirae* V_1-ATPase, J. Biol. Chem. 288 (2013) 32700–32707.
[75] G. Grüber, V. Marshansky, New insights into structure–function relationships between archeal ATP synthase (A_1A_O) and vacuolar type ATPase (V_1V_O), Bioessays 30 (2008) 1096–1109.
[76] A.G. Stewart, M. Sobti, R.P. Harvey, D. Stock, Rotary ATPases: models, machine elements and technical specifications, Bioarchitecture 3 (2013) 2–12.
[77] L.K. Lee, A.G. Stewart, M. Donohoe, R.A. Bernal, D. Stock, The structure of the peripheral stalk of *Thermus thermophilus* H^+-ATPase/synthase, Nat. Struct. Mol. Biol. 17 (2010) 373–378.
[78] A.M. Balakrishna, M.S. Manimekalai, C. Hunke, S. Gayen, M. Rössle, J. Jeyakanthan, G. Grüber, Crystal and solution structure of the C-terminal part of the *Methanocaldococcus jannaschii* A_1A_O ATP synthase subunit E revealed by X-ray diffraction and small-angle X-ray scattering, J. Bioenerg. Biomembr. 42 (2010) 311–320.
[79] A.M. Balakrishna, C. Hunke, G. Grüber, The structure of subunit E of the *Pyrococcus horikoshii* OT3 A-ATP synthase gives insight into the elasticity of the peripheral stalk, J. Mol. Biol. 420 (2012) 155–163.
[80] A.G. Stewart, L.K. Lee, M. Donohoe, J.J. Chaston, D. Stock, The dynamic stator stalk of rotary ATPases, Nat. Commun. 3 (2012) 687.
[81] S. Srinivasan, N.K. Vyas, M.L. Baker, F.A. Quiocho, Crystal structure of the cytoplasmic N-terminal domain of subunit I, a homolog of subunit *a*, of V-ATPase, J. Mol. Biol. 412 (2011) 14–21.
[82] V. Müller, An exceptional variability in the motor of archaeal A_1A_O ATPases: from multimeric to monomeric rotors comprising 6–13 ion binding sites, J. Bioenerg. Biomembr. 36 (2004) 115–125.
[83] K. Ihara, S. Watanabe, K. Sugimura, Y. Mukohata, Identification of proteolipid from an extremely halophilic archaeon *Halobacterium salinarum* as an N′, N′-dicyclohexyl-carbodiimide binding subunit of ATP synthase, Arch. Biochem. Biophys. 341 (1997) 267–272.
[84] K.I. Inatomi, M. Maeda, M. Futai, Dicyclohexylcarbodiimide-binding protein is a subunit of the *Methanosarcina barkeri* ATPase complex, Biochem. Biophys. Res. Commun. 162 (1989) 1585–1590.
[85] K. Steinert, V. Wagner, P.G. Kroth-Pancic, S. Bickel-Sandkötter, Characterization and subunit structure of the ATP synthase of the halophilic archaeon *Haloferax volcanii* and organization of the ATP synthase genes, J. Biol. Chem. 272 (1997) 6261–6269.
[86] F. Mayer, V. Leone, J.D. Langer, J.D. Faraldo-Gómez, V. Müller, A *c* subunit with four transmembrane helices and one ion (Na^+) binding site in an archaeal ATP synthase: implications for *c* ring function and structure, J. Biol. Chem. 287 (2012) 39327–39337.
[87] C. Ruppert, R. Schmid, R. Hedderich, V. Müller, Selective extraction of subunit D of the Na^+-translocating methyltransferase and subunit *c* of the A_1A_O ATPase from the cytoplasmic membrane of methanogenic archaea by chloroform/methanol and characterization of subunit *c* of *Methanothermobacter thermoautotrophicus* as a 16-kDa proteolipid, FEMS Microbiol. Lett. 195 (2001) 47–51.
[88] W.F. Fricke, H. Seedorf, A. Henne, M. Kruer, H. Liesegang, R. Hedderich, G. Gottschalk, R.K. Thauer, The genome sequence of *Methanosphaera stadtmanae* reveals why this human intestinal archaeon is restricted to methanol and H_2 for methane formation and ATP synthesis, J. Bacteriol. 188 (2006) 642–658.
[89] C. Ruppert, H. Kavermann, S. Wimmers, R. Schmid, J. Kellermann, F. Lottspeich, H. Huber, K.O. Stetter, V. Müller, The proteolipid of the A_1A_O ATP synthase from *Methanococcus jannaschii* has six predicted transmembrane helices but only two proton-translocating carboxyl groups, J. Biol. Chem. 274 (1999) 25281–25284.
[90] A.I. Slesarev, K.V. Mezhevaya, K.S. Makarova, N.N. Polushin, O.V. Shcherbinina, V.V. Shakhova, G.I. Belova, L. Aravind, D.A. Natale, I.B. Rogozin, R.L. Tatusov, Y.I. Wolf, K.O. Stetter, A.G. Malykh, E.V. Koonin, S.A. Kozyavkin, The complete genome of hyperthermophile *Methanopyrus kandleri* AV19 and monophyly of archaeal methanogens, Proc. Natl. Acad. Sci. U. S. A. 99 (2002) 4644–4649.
[91] D. Pogoryelov, A.L. Klyszejko, G.O. Krasnoselska, E.M. Heller, V. Leone, J.D. Langer, J. Vonck, D.J. Müller, J.D. Faraldo-Gómez, T. Meier, Engineering rotor ring stoichiometries in the ATP synthase, Proc. Natl. Acad. Sci. U. S. A. 109 (2012) E1599–E1608.
[92] F.T. Robb, D.L. Maeder, J.R. Brown, J. DiRuggiero, M.D. Stump, R.K. Yeh, R.B. Weiss, D.M. Dunn, Genomic sequence of hyperthermophile *Pyrococcus furiosus*: implications for physiology and enzymology, Methods Enzymol. 330 (2001) 134–157.
[93] D. Pogoryelov, O. Yildiz, J.D. Faraldo-Gómez, T. Meier, High-resolution structure of the rotor ring of a proton-dependent ATP synthase, Nat. Struct. Mol. Biol. 16 (2009) 1068–1073.
[94] P. Dimroth, Structure and function of the Na^+-translocating ATPase of *Propionigenium modestum*, Acta Physiol. Scand. 146 (1992) 97–102.
[95] V. Müller, S. Aufurth, S. Rahlfs, The Na^+ cycle in *Acetobacterium woodii*: identification and characterization of a Na^+-translocating F_1F_O-ATPase with a mixed oligomer of 8 and 16 kDa proteolipids, Biochim. Biophys. Acta 1505 (2001) 108–120.
[96] T. Murata, I. Yamato, Y. Kakinuma, A.G. Leslie, J.E. Walker, Structure of the rotor of the V-Type Na^+-ATPase from *Enterococcus hirae*, Science 308 (2005) 654–659.
[97] T. Meier, A. Krah, P.J. Bond, D. Pogoryelov, K. Diederichs, J.D. Faraldo-Gómez, Complete ion-coordination structure in the rotor ring of Na^+-dependent F-ATP synthases, J. Mol. Biol. 391 (2009) 498–507.
[98] T. Meier, P. Polzer, K. Diederichs, W. Welte, P. Dimroth, Structure of the rotor ring of F-Type Na^+-ATPase from *Ilyobacter tartaricus*, Science 308 (2005) 659–662.
[99] D.G. McMillan, S.A. Ferguson, D. Dey, K. Schroder, H.L. Aung, V. Carbone, G.T. Attwood, R.S. Ronimus, T. Meier, P.H. Janssen, G.M. Cook, A_1A_O-ATP synthase of *Methanobrevibacter ruminantium* couples sodium ions for ATP synthesis under physiological conditions, J. Biol. Chem. 286 (2011) 39882–39892.
[100] K. Schlegel, V. Leone, J.D. Faraldo-Gomez, V. Müller, Promiscuous archaeal ATP synthase concurrently coupled to Na^+ and H^+ translocation, Proc. Natl. Acad. Sci. U. S. A. 109 (2012) 947–952.
[101] S. Schulz, M. Iglesias-Cans, A. Krah, O. Yildiz, V. Leone, D. Matthies, G.M. Cook, J.D. Faraldo-Gomez, T. Meier, A new type of Na^+-driven ATP synthase membrane rotor with a two-carboxylate ion-coupling motif, PLoS Biol. 11 (2013) e1001596.
[102] N. Lane, W.F. Martin, The origin of membrane bioenergetics, Cell 151 (2012) 1406–1416.
[103] A.Y. Mulkidjanian, P. Dibrov, M.Y. Galperin, The past and present of sodium energetics: may the sodium-motive force be with you, Biochim. Biophys. Acta 1777 (2008) 985–992.
[104] A. Poehlein, S. Schmidt, A.-K. Kaster, M. Goenrich, J. Vollmers, A. Thürmer, J. Bertsch, K. Schuchmann, B. Voigt, M. Hecker, R. Daniel, R.K. Thauer, G. Gottschalk, V. Müller, An ancient pathway combining carbon dioxide fixation with the generation and utilization of a sodium ion gradient for ATP synthesis, PLoS One 7 (2012) e33439.